ADVANCED MATERIALS
www.advmat.de

Programming 3D Curves with Discretely Constrained Cylindrical Inflatables

Robert Baines, Sree Kalyan Patiballa, Benjamin Gorissen, Katia Bertoldi, and Rebecca Kramer-Bottiglio**

Programming inflatable systems to deform to desired 3D shapes opens up multifarious applications in robotics, morphing architecture, and interventional medicine. This work elicits complex deformations by attaching discrete strain limiters to cylindrical hyperelastic inflatables. Using this system, a method is presented to solve the inverse problem of programming myriad 3D centerline curves upon inflation. The method entails two steps: first, a reduced-order model generates a conceptual solution giving coarse indications of strain limiter placement on the undeformed cylindrical inflatable. This low-fidelity solution then seeds a finite element simulation nested within an optimization loop to further tune strain limiter parameters. We leverage this framework to achieve functionality through a priori programmed deformations of cylindrical inflatables, including 3D curve matching, self-tying knotting, and manipulation. The results hold broad significance for the emerging computational design of inflatable systems.

1. Introduction

The potential of inflatable systems to assume complex shapes and interact adaptively with their environment has propelled them to the forefront of next-generation soft robotics, deployable structures, and medical devices.[1–3] Critical interest has thus emerged regarding the inverse design of inflatables and other shape-morphing systems—specifying a deformation, and solving for the design parameters, that is geometric and/or material parameters, required to achieve this deformation.[4–9] Inverse design can reduce prototyping time, material waste, and results in more performant soft systems. Many inverse inflatable models have focused on systems composed of materials with a high elastic modulus (making them quasi-inextensible at operating pressure). This hardware choice reduces the modeling challenge yet limits the scope of achievable deformations.[10–13]

Inflatables composed of hyperelastic material can accommodate large strains, disposing them to applications requiring radical shape changes or large forces.[14–19] Hyperelastic inflatables commonly incorporate stiffer material strain limiters, including mesh, directional fibers, slotted shells, or varying-modulus rubber on their surface to direct deformations.[20–23] Simpler deformations like contraction or extension are well-studied and can be designed a priori with reduced force or energy-based models.[24–26] Models like these assume homogeneous deformations throughout the system, induced by a single strain limiter on an inflatable undergoing typically small (<40%), planar, and axisymmetric deformations. Similarly, models for specification of curvatures are capable of programming only planar curves and have been demonstrated with unidirectionally extending cylinders.[27]

Deformable systems that can inflate into non-homogeneous 3D forms open a more expansive application space. In these more complex emerging systems, the energetic interplay between locally stretched surface regions may give rise to topography with applications in mechanical camouflage and precision haptic devices,[28,29] or sinuous 3D curves with applications in continuum manipulation.[30] Localized strain-limiting entails boundary effects arising from material compliance mismatch that raise the required fidelity of a model to capture the deforming inflatable's mechanical response.

Finite element (FE) analysis has been shown to reliably predict the behavior of 3D inflating continua outfitted in discrete strain limiters.[31] FE simulation has recently been used for inverse design using neural networks to produce surfaces that inflate to programmed 3D topography.[32] Design strategies reliant entirely on machine learning however suffer from high computational expense, which can preclude their unaccompanied implementation in large-scale inverse design problems or transferability to systems composed of different materials.

R. Baines, S. K. Patiballa, R. Kramer-Bottiglio
School of Engineering and Applied Sciences
Yale University
CT 06511New Haven, USA
E-mail: robert.baines@yale.edu; rebecca.kramer@yale.edu
S. K. Patiballa
Department of Mechanical Engineering
The University of Alabama
AL 35487Tuscaloosa, USA
B. Gorissen, K. Bertoldi
J. A. Paulson School of Engineering and Applied Sciences
Harvard University
MA 02138Cambridge, USA
B. Gorissen
Department of Mechanical Engineering
KU Leuven
Celestijnenlaan 300, Leuven3001, Belgium

The ORCID identification number(s) for the author(s) of this article can be found under https://doi.org/10.1002/adma.202300535

DOI: 10.1002/adma.202300535

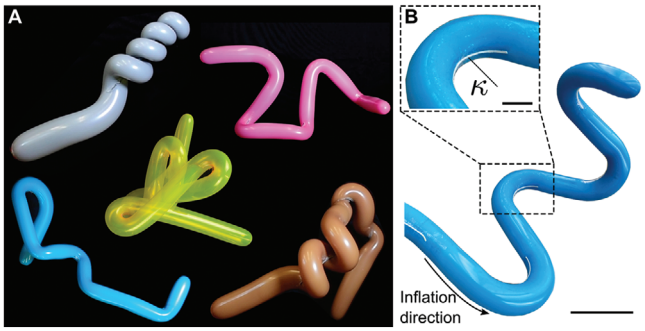

Figure 1. Adhering discrete strain-limiting patches to the surface of hyperelastic inflatable cylinders gives rise to complex and functional forms. A) Several inflatables fabricated using this technique are shown. B) Image of prototype inflatable with patches that influence curvature κ and torsion τ in extremely non-linear ways based on their dimensions, orientation, and placement along the continuum surface. The zoomed inset shows how even a localized 1 mm-wide, 4 cm-long patch can produce curvature that substantially changes the global morphology of an inflatable at the meter scale (Inset scale bar: 2 cm; Image scale bar: 15 cm). We propose an inverse design pipeline to yield strain limiter design parameters for an uninflated cylinder such that when inflated, its centerline matches a user-input space curve.

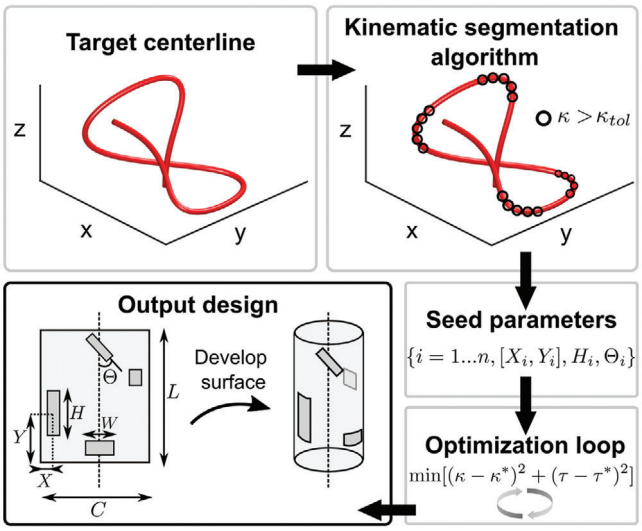

Figure 2. Visual depiction of inverse design pipeline, starting with a target centerline going into kinematic segmentation algorithm, the solution of which is in turn used to seed a FE simulation nested within an optimization loop. The output of this pipeline are strain limiter design parameters to match a target centerline.

Despite recent progress, there is still a dearth of inverse design models for 3D discretely constrained inflatables, which acts as a bottleneck to adopting multifunctional soft systems in critical application spaces. This fact motivates a framework capable of capturing nuanced mechanics for solution accuracy yet able to generate conceptual solutions in reduced time. Here, we present such a framework and evaluate it by focusing on a useful, albeit relatively unexplored case of elongated inflated cylinders clad in discrete strain-limiting "patches." The number, dimensions, locations, and orientations of patches placed on the cylinder may be tuned to coerce myriad space curves (**Figure 1**, Video 1, Supporting Information), with applications ranging from shape matching, manipulation, navigation, to self-tying knots. Our inverse method solves for patch design parameters to be placed on an uninflated cylinder such that the centerline of the inflated cylinder closely approximates a user-input space curve.

Starting with a user-input space curve ($C \in \mathbb{R}^3$), we use kinematics to generate a conceptual solution for strain limiter placement and heights on the uninflated geometry. Next, the conceptual solution seeds an FE simulation nested within an optimization structure that tunes strain limiter placement and dimensions. The conceptual solution emerges from a reduced-order model that provides intuition about the mechanics that govern elongate hyperelastic inflatables clad in discrete strain limiters; furthermore, seeding the FE optimization loop with this conceptual solution reduces the design search space, facilitating faster convergence on valid parameters than using FE alone.

2. Results and Discussion

Rectangular strain-limiting patches $i = 1 \ldots n$ with dimensions $H_i \times W_i$ are placed on an undeformed cylindrical inflatable of length L at positions $[X_i, Y_i]$ (on the developable surface), and angles with respect to the longitudinal axis Θ_i (**Figure 2**). Upon inflation, the inflatable undergoes large extensional and radial stretches while the patches influence curvature (κ) and torsion (τ) of the centerline parameterized by arclength t (see Figure S1, Supporting Information, for fabrication of inflatables and a typical pressure–volume curve). Herein, we strive to model the relationship between patch placement and $\kappa(t)$ and $\tau(t)$ to systematically program curves.

The inflation of patch-clad cylindrical inflatables is characterized by multiple snap-through instabilities. The first of these instabilities is associated with the inflatable reaching a critical pressure and developing an initial bulge.[33] Subsequent snap-troughs arise from overcoming local stiffness discontinuities due to the presence of patches.[34] Once the air bulge has propagated to the cylinder's distal tip, the inflatable assumes its fully inflated shape. This state of static equilibrium during the first inflation cycle, in which curvature caused by patches is fully "activated," is the concern in this work (see Note S1, Supporting Information, for more discussion on inflation mechanics of patch-clad inflatables).

2.1. Kinematic Segmentation Algorithm

The first part of our inverse design pipeline is a conceptual solution, enabled by a reduced-order model, which we dub "kinematic segmentation algorithm" (KSA). Given a target curve C, KSA quickly generates coarse estimates of n, ($[X_i, Y_i]$), H_i, and Θ_i along an uninflated cylinder, overlooking complexities arising from material properties. The advantage of KSA is twofold: it provides insight into the mechanics of the deforming cylinder and an initial guess for the FE optimization loop to reduce convergence time due to the highly non-convex search space.

In KSA, first, a discrete Frenet–Serret triad consisting of the tangent $\bar{T}$, normal $\bar{N}$, and binormal $\bar{B}$ triad, is calculated for C. We then identify where curvature ($\kappa = ||d\bar{T}/dl||$) exceeds a predefined threshold κ_{tol} (Note S2, Supporting Information). If a point exceeds κ_{tol}, we ascribe that point along the arclength to

have a patch. Close-by segments within a specified tolerance are merged, and the axial midpoints of the resulting sections deemed to have a patch are calculated, indicating the axial midpoint of a patch in the deformed configuration, γ_i. Knowing the initial length of an uninflated cylinder and the length of a target centerline (L_f), we calculate the axial stretch $\lambda = L_f/L$ and then find the patch axial midpoint in the reference configuration $Y_i = \gamma_i/\lambda$. H_i is estimated as the length of the segments that exceed κ_{tol}. We estimate X_i using the angle of twist of $\bar{B}$ along the curve up to a midpoint of a segment. Similarly, we estimate Θ_i by calculating the angle of twist of $\bar{B}$ through a segment and assuming the patch angle in the undeformed configuration maps directly to the centerline twist it exerts in the deformed configuration. Although it rapidly yields a conceptual solution, KSA alone does not furnish a complete solution because it does not estimate the width of the patches W_i. The influence of patch parameters on κ and τ depends on the patch's material properties, and the boundary effects between the patch and the inflated cylinder. Both of these considerations require a model beyond the simplified kinematic representation.

2.2. Finite Element Model

An FE simulation nested within an optimization loop constitutes the second part of the inverse design pipeline. The FE simulations (which were conducted using the commercial package ABAQUS 2020/Explicit) account for the mechanical boundary effects and material properties omitted from KSA through nonlinear elasticity; they model the cylindrical inflatable and patches as isotropic membrane elements governed by hyperelastic constitutive laws (Note S3, Supporting Information). We performed forward validations to ensure the accuracy of the FE model (Note Figure S2 and S4, Supporting Information).

In the inverse FE problem, a shape-matching objective is formulated as a minimization of the squared difference between target and simulation torsion and curvature:

$$\min_{X_i, Y_i, H_i, W_i, \Theta_i} \left(\kappa(t) - \kappa(t)^*\right)^2 + \left(\tau(t) - \tau(t)^*\right)^2 \quad (1)$$

$$\text{s.t}: Lb_i \leq \left(X_i, Y_i, H_i, W_i, \sqrt{}_i\right) \leq Ub_i \quad (2)$$

Here, * denotes the target values. An optimal solution is computed by searching the design space while satisfying the constraints (bounds on reasonable sizes of patches, denoted as Lb_i through Ub_i; see Note S5, Supporting Information). Due to the non-convex search space of the optimization problem and the number of free variables, we chose an evolutionary algorithm known as the "co-variance matrix adaptation evolution strategy" (CMA-ES), which is well-suited to such problems.[35]

2.3. Assessment of Inverse Design Pipeline

We evaluated the inverse design pipeline with four input curves (**Figure 3**A–D): Hilbert's space-filling curve [36] (which is not traditionally differentiable, but we use a smooth approximation), two bespoke 3D curves, and an equation-driven curve describing the contour of a hyperbolic paraboloid (Note S6, Supporting Information). We crafted inflatables according to the output of the inverse design pipeline by laser cutting patches and adhering them to the surface of the inflatable. Then, after inflation, we took a 3D scan of the inflatable from which the centerline was extracted (Note S7 and Figure S3, Supporting Information).

Results testify that the inverse design pipeline can accurately generate valid design parameters to approximate a variety of space curves with diverse torsion and curvature profiles. Due to the different lengths of target and experimental centerlines, we used dynamic time warping [37] to quantitatively evaluate similarity (an explanation of dynamic time warping, as well as its value for each curve's torsion and curvature as a function of arclength are tabulated in Note S6, Supporting Information). Calculations yielded a value averaged over all curves of 0.5887 for curvature, and 1.4899 for torsion.

The patch-clad inflatables' successful replication of certain target curve features, while difficulty in replicating others, elucidates general design considerations for elongate hyperelastic systems clad in discrete, distributed strain limiters. From the similarity metric provided by dynamic time warping, we remark that torsion approximation was less accurate than curvature approximation. Additionally, sharp peaks in curvature or torsion over relatively small distances in arclength prove difficult, owing to the inability of the inflatable to produce true inflection points or twist very rapidly. This challenge is embodied in the Hilbert curve of Figure 3A, which does not consistently reach the full extent of target curvature and torsion. Another apparent challenge is maintaining constant κ or τ over a sizable span of arclength. For instance, the inflatable centerline in Figure 3B does not maintain constant κ at each peak. Likewise, Figure 3C has small fluctuations in κ that prevent it from tracking the smooth dip and rise of the target curve.

We ascertained the performance of the FE simulation alone and when it was seeded with KSA in generating designs for Figure 3C. Results show that KSA generates nearby solution guesses for the patch parameters, limiting the FE search space in the otherwise rugged energy landscape, and reducing the number of required iterations to converge on designs which minimize the objective in Equations (1) and (2) (Note S8 and Figure S4, Supporting Information).

2.4. Applications

Equipped with the inverse design framework, we showcase how an inflated shape can be harnessed for robotic functionality beyond mere curve matching. First, we created a self-tying knot (Figure 4A, Video S2, Supporting Information), an application necessitating both highly curved deformations and nonhomogeneous inflation, due to the intersections that are present when mapping the undeformed to the deformed deformation. Due to a base-to-tip inflation,[38] the inflatable experiences no self-intersection until it is deflated and the retraction force tightens the knot. We envision programmable self-tying knots with a single input volume that could be used in medicinal applications, to staunch blood flow, or in deployable structures to rapidly create architectural fixtures.

Additionally, we demonstrated programmable grasping of various objects across different length scales using unusual

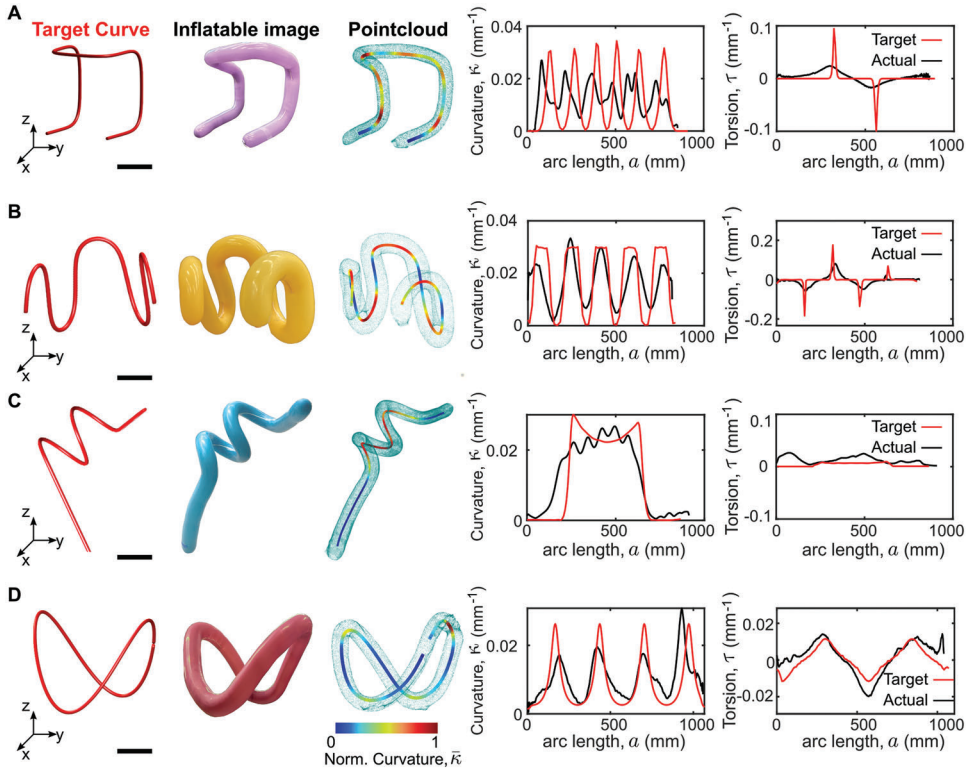

Figure 3. Benchmark target centerlines used in assessing the KSA-FE optimization pipeline. The curves span a variety of different curvature and torsion profiles as a function of arclength. For each we show the resulting inflatable and a 3D pointcloud of the inflatable with a juxtaposed centerline indicating magnitude of curvature. A) Smooth version of Hilbert's space-filling curve. Scale bar: 8 cm. B,C) Hand-drawn curves. Scale bars: 11.5 and 7.5 cm, respectively. D) Equation that describes the contour of a hyperbolic paraboloid surface. Scale bar: 10 cm.

continuum grasp modes (Figure 4B–E, Video S3, Supporting Information). Programmed helix diameters or hooking curvatures also enabled the inflatable to manipulate multiple objects at once. For instance, tight helices were able to pinch and lift small-diameter objects, like the nozzle of a soap dispenser (Figure 4B), whereas looser helices served as a power grasp to extract and subsequently return objects of greater diameter, like plastic pipes, in a recycling bin (Figure 4C). Multi-object grasping was accomplished by programming distributed functional torsion and curvature across the inflatable length. As examples, with an inflatable consisting of a single volume, we ensnared and lifted two buckets (Figure 4D), or encoded helices and hooks to retrieve disparately shaped objects—a pipe and a metallic fixture—from a recycling bin (Figure 4E). Ultimately, multiple dissimilar object grasping is viable with the elongate inflatables and holds promise for robotic manipulation applications.

3. Conclusion

The burgeoning field of soft robotics is rife with soft actuation technologies that expand the bounds of what is possible in robotic functionality. Applying strain limiters to the surface of soft volumetrically expanding bodies makes it possible to elicit intricate 3D shapes. Despite the ability to easily create them, there is a distinct lack of principled design methods for these highly nonlinear soft deforming bodies.

With elongated cylindrical systems clad in discrete strain limiters as a model system, we present an inverse design method that elicits strain limiter parameters required to match target 3D curves. Programming myriad 3D curves is enabled by the proposed modeling pipeline (akin to initial-guess generation techniques [39,40]) that seeds a high-fidelity FE model with a conceptual solution resulting in a decrease in iterations required to reach desired levels of objective fitness. Moreover, in inverse design, FE can often act as a black box, obfuscating intuition of the design solution,[41,42] which motivates a reduced-order model to provide intuition to the designer. We quantitatively evaluated the efficacy of shape matching with several benchmark curves of varying curvature and torsion profiles, and subsequently demonstrated how inflation to programmed 3D curves can be harnessed to interact dexterously in the environment with a single pressurized volume.

There are many exciting avenues related to this study to explore. For instance, a rich design space is available when patch directional moduli are left as a free parameter in the optimization. Novel shapes could be achievable when the patch geometry is not constrained to a rectangle but left to vary. Another remaining challenge is to study how trajectories change under dynamic inflation rather than in quasi-static equilibrium manifolds. Lastly, considering self-contact in the model would expand utility to applications with specified force requirements. In the interest of reducing prototyping time, material waste, and stepping toward optimal performance, we anticipate such an inverse design method

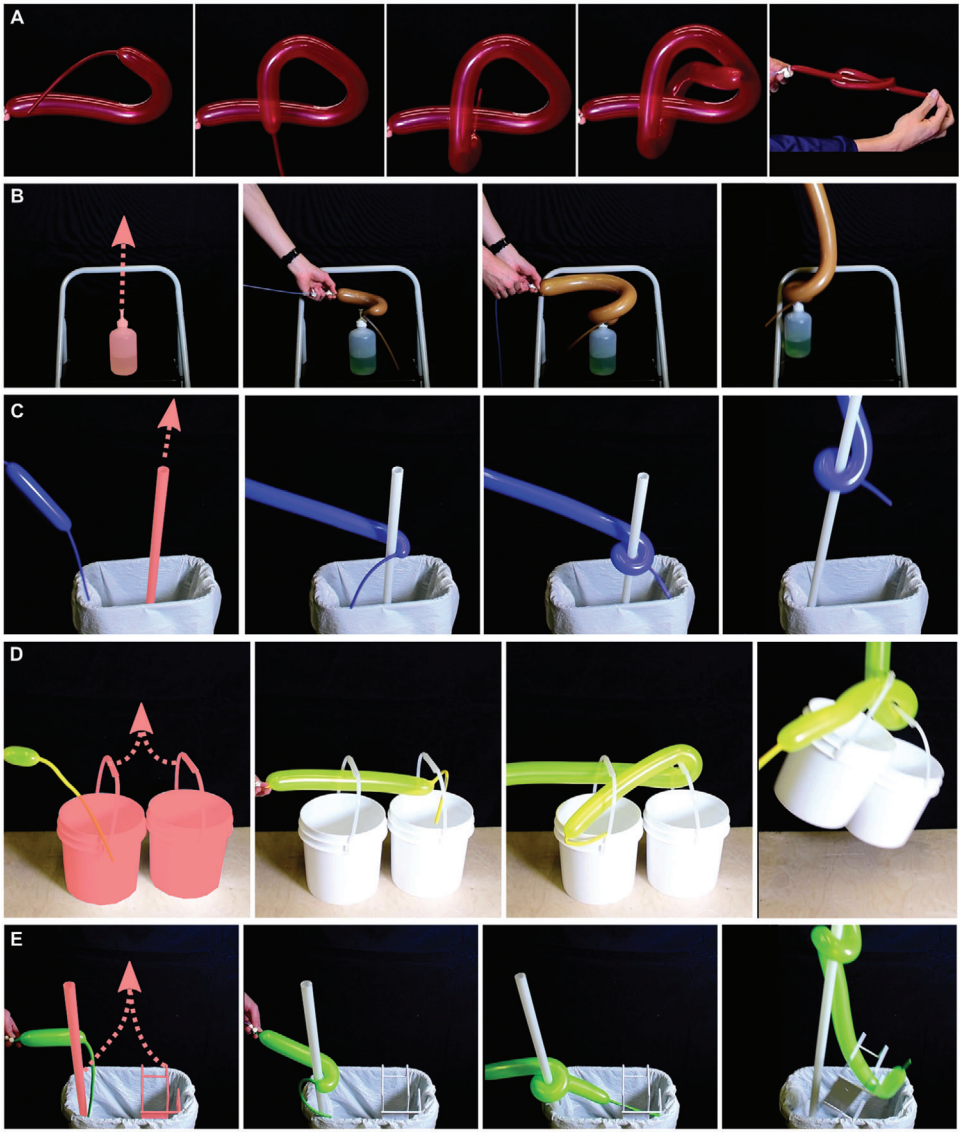

Figure 4. Applications. A single volumetrically inflating cylinder clad in discrete strain-limiting patches can accomplish highly dexterous functions. A) Self-tying knot. B) Grasping and lifting a bottle by a 10 mm diameter nozzle using a tight helix. C) Grasping and lifting a PVC pipe of diameter 40 mm using a helix with larger radius. D) Simultaneous grasping and lifting of two buckets by exploiting a loop knot. E) Grasping multiple differently shaped objects using a combination of enveloping and hinge grasps.

could be applied to various other soft systems where modeling has proven a challenge: soft robotics, smart structures, or more generally, any field in which inverse design of 3D inflatables may be applicable (Note S9, Supporting Information).

4. Experimental Section

To make strain-limiting patches, Spandex (Polyester Lycra/Spandex four-way stretch fabric LY 902, Paylessfabric) was dredged in Liquid Latex (Kangaroo Monster Liquid Latex) and allowed to cure for 24 h. Patch dimensions were drawn as a DXF file and cut from the spandex composite with a laser cutter (Universal Laser Systems, VLS 2.3). Then, rubber cement (BestTest White Paper Cement, Bestine) served to adhere the patch to the cylindrical inflatable (Qualtex 260d balloons), essentially solvent welding the latex-infused spandex patch to the latex surface. To ensure complete cure and maximum adhesion waiting was done for 24 h before inflating. Please see Supporting Information for more details about experiments and simulations.

Supporting Information

Supporting Information is available from the Wiley Online Library or from the author.

Acknowledgements

The authors thank Dr. Gaurav Singh for thought-provoking discussions, and labmates for accommodating guerilla balloon art installations on the

benchtops for several months. This project was sponsored by the Office of Naval Research under award N00014-21-1-2417. Any opinions, findings, and conclusions or recommendations expressed in this material were those of the authors and do not necessarily reflect the views of the Office of Naval Research. R.B. was supported by the NSF Graduate Research Fellowship Program (DGE-1752134)

Conflict of Interest

The authors declare no conflict of interest.

Data Availability Statement

All data needed to evaluate the conclusions in the paper are present in the paper and/or the Supporting Information. Additional data related to this paper are available from the authors upon request. Design pipeline scripts can be downloaded at https://github.com/thefaboratory/3d_discrete_inflatables.

Keywords

inflatables, inverse design, programmable matter, soft actuators, soft robotics

Received: January 17, 2023
Revised: March 17, 2023
Published online:

[1] E. Siéfert, M. Warner, *Proc. R. Soc. A* **2020**, *476*, 20200047.
[2] E. W. Hawkes, L. H. Blumenschein, J. D. Greer, A. M. Okamura, *Sci. Rob.* **2017**, *2*, eaan3028.
[3] Y.-J. Kim, S. Cheng, S. Kim, K. Iagnemma, *IEEE Trans. Rob.* **2013**, *29*, 1031.
[4] E. Siéfert, E. Reyssat, J. Bico, B. Roman, *Nat. Mater.* **2019**, *18*, 24.
[5] D. Melancon, B. Gorissen, C. J. García-Mora, C. Hoberman, K. Bertoldi, *Nature* **2021**, *592*, 545.
[6] A. S. Gladman, E. A. Matsumoto, R. G. Nuzzo, L. Mahadevan, J. A. Lewis, *Nat. Mater.* **2016**, *15*, 413.
[7] T. J. Jones, E. Jambon-Puillet, J. Marthelot, P.-T. Brun, *Nature* **2021**, *599*, 229.
[8] D. Jiao, Q. L. Zhu, C. Y. Li, Q. Zheng, Z. L. Wu, *Acc. Chem. Res.* **2022**, *55*, 1533.
[9] H. Aharoni, Y. Xia, X. Zhang, R. D. Kamien, S. Yang, *Proc. Natl. Acad. Sci. USA* **2018**, *115*, 7206.
[10] E. Siéfert, E. Reyssat, J. Bico, B. Roman, *Proc. Natl. Acad. Sci. USA* **2019**, *116*, 16692.
[11] M. Skouras, B. Thomaszewski, P. Kaufmann, A. Garg, B. Bickel, E. Grinspun, M. Gross, *ACM Trans. Graphics* **2014**, *33*, 1.
[12] J. Panetta, F. Isvoranu, T. Chen, E. Siéfert, B. Roman, M. Pauly, *ACM Trans. Graphics* **2021**, *40*, 1.
[13] R. Baines, S. Patiballa, R. Kramer-Bottiglio, in *2021 IEEE 4th Int. Conf. on Soft Robotics (RoboSoft)*, IEEE, Piscataway, NJ, USA **2021**, pp. 29–34.
[14] N. El-Atab, R. B. Mishra, F. Al-Modaf, L. Joharji, A. A. Alsharif, H. Alamoudi, M. Diaz, N. Qaiser, M. M. Hussain, *Adv. Intell. Syst.* **2020**, *2*, 2000128.
[15] J. C. Case, E. L. White, R. K. Kramer, *Soft Rob.* **2015**, *2*, 80.
[16] A. Miriyev, K. Stack, H. Lipson, *Nat. Commun.* **2017**, *8*, 596.
[17] S. A. Morin, R. F. Shepherd, S. W. Kwok, A. A. Stokes, A. Nemiroski, G. M. Whitesides, *Science* **2012**, *337*, 828.
[18] N. G. Kim, J.-H. Ryu, *Adv. Intell. Syst.* **2022**, *5*, 2200264.
[19] K. Althoefer, *Nat. Rev. Mater.* **2018**, *3*, 76.
[20] C.-P. Chou, B. Hannaford, *IEEE Trans. Rob. Autom.* **1996**, *12*, 90.
[21] F. Connolly, C. J. Walsh, K. Bertoldi, *Proc. Natl. Acad. Sci. USA* **2017**, *114*, 51.
[22] L. Belding, B. Baytekin, H. T. Baytekin, P. Rothemund, M. S. Verma, A. Nemiroski, D. Sameoto, B. A. Grzybowski, G. M. Whitesides, *Adv. Mater.* **2018**, *30*, 1704446.
[23] R. V. Martinez, J. L. Branch, C. R. Fish, L. Jin, R. F. Shepherd, R. M. Nunes, Z. Suo, G. M. Whitesides, *Adv. Mater.* **2013**, *25*, 205.
[24] J. Bishop-Moser, S. Kota, *IEEE Trans. Rob.* **2015**, *31*, 536.
[25] G. Singh, G. Krishnan, *Smart Mater. Struct.* **2017**, *26*, 065024.
[26] A. Sedal, D. Bruder, J. Bishop-Moser, R. Vasudevan, S. Kota, *J. Mech. Rob.* **2018**, *10*, 024501.
[27] G. Singh, G. Krishnan, *Soft Rob.* **2019**, *7*, 109.
[28] J. Pikul, S. Li, H. Bai, R. Hanlon, I. Cohen, R. Shepherd, *Science* **2017**, *358*, 210.
[29] W. M. van Rees, E. A. Matsumoto, A. S. Gladman, J. A. Lewis, L. Mahadevan, *Soft Matter* **2018**, *14*, 8771.
[30] B. Yang, R. Baines, D. Shah, S. Patiballa, E. Thomas, M. Venkadesan, R. Kramer-Bottiglio, *Sci. Adv.* **2021**, *7*, eabh2073.
[31] S. Y. Kim, R. Baines, J. Booth, N. Vasios, K. Bertoldi, R. Kramer-Bottiglio, *Nat. Commun.* **2019**, *10*, 1.
[32] A. E. Forte, P. Z. Hanakata, L. Jin, E. Zari, A. Zareei, M. C. Fernandes, L. Sumner, J. Alvarez, K. Bertoldi, *Adv. Funct. Mater.* **2022**, *32*, 2111610.
[33] S. Kyriakides, C. Yu-Chung, *Int. J. Solids Struct.* **1991**, *27*, 1085.
[34] J. T. B. Overvelde, T. Kloek, J. J. A. D'haen, K. Bertoldi, *Proc. Natl. Acad. Sci. USA* **2015**, *112*, 10863.
[35] N. Vasios, A. J. Gross, S. Soifer, J. T. Overvelde, K. Bertoldi, *Soft Rob.* **2020**, *7*, 1.
[36] H. Sagan, *Space-Filling Curves*, Springer, Berlin, Germany, **1994**.
[37] D. J. Berndt, J. Clifford, in *AAAIWS'94: Proc. 3rd Int. Conf. on Knowledge Discovery and Data Mining*, ACM, New York **1994**, pp. 359–370.
[38] I. Müller, P. Strehlow, *Rubber and Rubber Balloons: Paradigms of Thermodynamics*, Lecture Notes in Physics, vol. *637*, Springer, Berlin, Germany, **2004**.
[39] L. Bayón, J. M. Grau, M. M. Ruiz, P. M. Suárez, *J. Math. Chem.* **2010**, *48*, 28.
[40] P. Tsiotras, E. Bakolas, Y. Zhao, in *AIAA Guidance, Navigation, and Control Conference*, American Institute of Aeronautics and Astronautics, Reston, VA, USA **2011**, https://doi.org/10.2514/6.2011-6689.
[41] S. K. Patiballa, G. Krishnan, *Mech. Based Des. Struct. Mach.* **2020**, *142*, 052310.
[42] Y. Bar-Sinai, G. Librandi, K. Bertoldi, M. Moshe, *Proc. Natl. Acad. Sci. USA* **2020**, *117*, 10195.